BNL -62295

PHASE TRANSFORMATION AND GROWTH OF HYGROSCOPIC AEROSOLS

I. N. Tang
Environmental Chemistry Division
Department of Applied Science
Brookhaven National Laboratory
Upton, NY 11973

September 1995

For publication as a Chapter in
Chemical Processes in Aerosols,
K. R. Spurny, Ed., CRC Lewis, Inc., Boca Raton, FL

This research was performed under the auspices of the U.S. Department of Energy under Contract No. DE-AC02-76CH00016.

DISCLAIMER

Portions of this document may be illegible in electronic image products. Images are produced from the best available original document.

Abstract

Ambient aerosols frequently contain large portions of hygroscopic inorganic salts such as chlorides, nitrates, and sulfates in either pure or mixed forms. Such inorganic salt aerosols exhibit the properties of deliquescence and efflorescence in air. The phase transformation from a solid particle to a saline droplet usually occurs spontaneously when the relative humidity of the atmosphere reaches a level specific to the chemical composition of the aerosol particle. Conversely, when the relative humidity decreases and becomes low enough, the saline droplet will evaporate and suddenly crystallize, expelling all its water content. The phase transformation and growth of aerosols play an important role in many atmospheric processes affecting air quality, visibility degradation, and climate changes. In this chapter, an exposition of the underlying thermodynamic principles is given, and recent advances in experimental methods utilizing single-particle levitation are discussed. In addition, pertinent and available thermodynamic data, which are needed for predicting the deliquescence properties of single and multi-component aerosols, are compiled. This chapter is useful to research scientists who are either interested in pursuing further studies of aerosol thermodynamics, or required to model the dynamic behavior of hygroscopic aerosols in a humid environment.

Contents

Introduction

Ambient aerosols play an important role in many atmospheric processes affecting air quality, visibility degradation, and climate changes as well. Both natural and anthropogenic sources contribute to the formation of ambient aerosols, which are composed mostly of sulfates, nitrates and chlorides in either pure or mixed forms. These inorganic salt aerosols are hygroscopic by nature and exhibit the properties of deliquescence and efflorescence in humid air. For pure inorganic salt particles with diameter larger than 0.1 micron, the phase transformation from a solid particle to a saline droplet occurs only when the relative humidity in the surrounding atmosphere reaches a certain critical level corresponding to the water activity of the saturated solution. The droplet size or mass in equilibrium with relative humidity can be calculated in a straightforward manner from thermodynamic considerations. For aqueous droplets 0.1 micron or smaller, the surface curvature effect on vapor pressure becomes important and the Kelvin equation must be used (La Mer and Gruen, 1952).

In reality, however, the chemical composition of atmospheric aerosols is highly complex and often varies with time and location. Junge (1952) has shown

that the growth of atmospheric aerosol particles in the continental air masses deviates substantially from what is predicted for the growth of pure salts. He explained this difference by assuming a mixture of soluble and insoluble material within the particle, thus introducing the concept of mixed nuclei for atmospheric aerosols. Subsequent investigation by Winkler (1973) has led to an empirical expression for the growth of continental atmospheric aerosol particles. Tang (1976) has considered the deliquescence and growth of mixed-salt particles, relating aerosol phase transformation and growth to the solubility diagrams for multicomponent electrolyte solutions.

In this Chapter, an exposition of the underlying thermodynamic principles on aerosol phase transformation and growth is given. Recent advances in experimental methods utilizing single-particle levitation are discussed. In addition, pertinent and available thermodynamic data, which are needed for predicting the deliquescence properties of single and multi-component aerosols, are compiled. Information on the composition and temperature dependence of these properties is required in mathematical models for describing the dynamic and transport behavior of ambient aerosols. Such data, however, are very scarce in the literature, especially when dealing with aerosols composed of mixed salts as an internal mixture.

Single-Particle Levitation Experiments

Numerous methods have been employed by investigators to study aerosol phase transition and growth in humid air. Thus, Dessens (1949) and Twomey (1954) conducted deliquescence experiments with both artificial salt and ambient

particles collected on stretched spider webs. They examined the particles with a microscope and noted phase transition in humid air. Orr *et al.* (1958) investigated the gain and loss of water with humidity change by measuring the change in electrical mobility for particles smaller than 0.1 μm. Winkler and Junge (1972) used a quartz microbalance and studied the growth of both artificial inorganic salt aerosols and atmospheric aerosol samples collected on the balance by impaction. Covert *et al.* (1972) also reported aerosol growth measurements using nephelometry. Finally, Tang et al. (1977) constructed a flow reactor with controlled temperature and humidity and measured the particle size changes of a monodisperse aerosol with an optical counter. Although these methods suffer from either possible substrate effects or some difficulties in accurate particle size and relative humidity measurements, they have provided information for a clear understanding of the hydration behavior of hygroscopic aerosols.

In recent years, however, new experimental techniques have been developed for trapping a single micron-sized particle in a stable optical or electrical potential well. These new techniques have made it possible to study many physical and chemical properties that are either unique to small particles or otherwise inaccessible to measurement with bulk samples. An earlier review by Davis (1983) documented the progress up to 1982. Since then, many interesting investigations have appeared in the literature. In particular, thermodynamic (Richardson and Spann, 1984; Tang et al. 1986; Cohen et al. 1987a) and optical properties (Tang and Munkelwitz, 1991; 1994a) of electrolyte solutions at concentrations far beyond saturation that could not have been achieved in the bulk, can now be measured

with a levitated microdroplet. This is accomplished by continuously and simultaneously monitoring the changes in weight and in Mie scattering patterns of a single suspended solution droplet undergoing controlled growth or evaporation in a humidified atmosphere, thereby providing extensive data over the entire concentration region. Other interesting works on the physics and chemistry of microparticles have been discussed in the recent review by Davis (1992). In this Section, the experimental methods used by Richardson and Kurtz (1984) and Tang et al. (1986) are described in some detail.

Single particle levitation is achieved in an electrodynamic balance (or quadrupole cell), whose design and operating principles have been described elsewhere (Straubel, 1956; Wueker et al., 1959; Frickel et al., 1978; Davis, 1985). Briefly, an electrostatically charged particle is trapped at the null point of the cell by an ac field imposed on a ring electrode surrounding the particle. The particle is balanced against gravity by a dc potential, U, established between two endcap electrodes positioned symmetrically above and below the particle. All electrode surfaces are hyperboloidal in shape and separated by Teflon insulators. When balanced at the null point, the particle mass, w, is given by

$$w = \frac{qU}{gz_o} \tag{1}$$

where q is the number of electrostatic charges carried by the particle, g the gravitational constant, and z_o the characteristic dimension of the cell. It follows that the relative mass changes, w/w_0, resulting from water vapor condensation or

evaporation can be measured as precisely as measurement of the dc voltage changes, U/U_0, that are necessary for restoring the particle to the null point. Here, the subscript, o, refers to measurements for the initial dry salt particle.

A schematic diagram of the apparatus is shown in Figure 1. The single-particle levitation cell is placed inside a vacuum chamber equipped with a water jacket that can maintain the cell temperature within ±0.1°C. A linear, vertically polarized He-Ne laser beam, entering the cell through a side window, illuminates the particle, 6-8 μm in diameter when dry. The particle position is continuously monitored by a CCD video camera and displayed on a TV screen for precise null point balance. The 90° scattered light is also continuously monitored with a photomultiplier tube. The laser beam, which is mechanically chopped at a fixed frequency, is focused on the particle so that a lock-in amplifier can be used to achieve high signal-to-noise ratios in the Mie scattering measurement.

Initially, a filtered solution of known composition is loaded in a particle gun; a charged particle is injected into the cell and captured in dry N_2 at the center of the cell by properly manipulating the ac and dc voltages applied to the electrodes. The system is closed and evacuated to a pressure below 10^{-7} torr. The vacuum is then valved off and the dc voltage required to position the particle at the null point is now noted as U_0. The system is then slowly back filled with water vapor during particle deliquescence and growth. Conversely, the system is gradually evacuated during droplet evaporation and efflorescence. The water vapor pressure, p_1, and the balancing dc voltage, U, are simultaneously recorded in pairs during the entire experiment. Thus, the ratio, U_0/U , represents the solute

mass fraction and the ratio, p_1/p_1°, gives the corresponding water activity, a_1, at that point. Here, p_1° is the vapor pressure of water at the system temperature. The measurement can be repeated several times with the same particle by simply raising the water vapor pressure again and repeating the cycle. The reproducibility is better than ±2%.

Hydration Behavior and Metastability

A deliquescent salt particle, such as KCl, NaCl, or a mixture of both, exhibits characteristic hydration behavior in humid air. Typical growth and evaporation cycles at 25°C are shown in Figure 2. Here, the particle mass change resulting from water vapor condensation or evaporation is plotted as a function of relative humidity (RH). Thus, as RH increases, a crystalline KCl particle (as illustrated by solid curves) remains unchanged (Curve A) until RH reaches its deliquescence point (RHD) at 84.3 %RH. Then, it deliquesces spontaneously (Curve B) to form a saturated solution droplet by water vapor condensation, gaining about 3.8 times its original weight. The droplet continues to grow as RH further increases (Curve C). Upon decreasing RH, the solution droplet loses weight by water evaporation. It remains a solution droplet even beyond its saturation point and becomes highly supersaturated as a metastable droplet (Curve D) at RH much lower than RHD. Finally, efflorescence occurs at about 62 %RH (Curve E), when the droplet suddenly sheds all its water content and becomes a solid particle. Similar behavior is illustrated in Figure 2 as dashed curves for a NaCl particle, which deliquesces at 75.4 %RH and crystallizes at about 48 %RH. Note that, for a single-salt particle, the particle is either a solid or a droplet, but not in

a state of partial dissolution.

In a bulk solution, crystallization always takes place not far beyond the saturation point. This happens because the presence of dust particles and the container walls invariably induces heterogeneous nucleation at a much earlier stage than what would be expected for homogeneous nucleation to occur. On the other hand, in a solution droplet where the presence of an impurity nucleus is rare, homogeneous nucleation normally proceeds at high supersaturations. Thus, the hysteresis shown in Figure 2 by either the KCl or NaCl particle represents a typical behavior exhibited by all hygroscopic aerosol particles. The observations reported by Rood et al.(1989) also revealed that in both urban and rural atmospheres, metastable droplets indeed existed more than 50% of the time when RH was between about 45 and 75%. Since solution droplets tend to become highly supersaturated before efflorescence, the resulting solid may be in a metastable state that is not predicted from the bulk-phase thermodynamic equilibrium. In fact, some solid metastable states formed in hygroscopic particles may not even exist in the bulk phase (Tang et al., 1995). It follows that the hydration properties of hygroscopic aerosol particles can not always be predicted from their bulk-solution properties.

A case of interest is Na_2SO_4 aerosol particles. In bulk solutions at temperatures below 35°C, sodium sulfate crystallizes with ten water molecules to form the stable solid phase decahydrate, $Na_2SO_4 \cdot 10H_2O$ (Seidell and Linke, 1965). In suspended microparticles, however, it is the anhydrous solid, Na_2SO_4, that is formed most frequently from the crystallization of supersaturated solution

droplets. This fact is established both by particle mass measurements (Cohen et al., 1987a) and by Raman spectroscopy (Tang et al., 1995). Fig. 3 shows the growth (open circles) and evaporation (filled circles) of a Na_2SO_4 particle in a humid environment at 25°C. The hydration behavior is qualitatively very similar to that of the KCl or NaCl particle shown in Fig. 2. Thus, as RH increases, an anhydrous Na_2SO_4 particle deliquesces at 84 %RH to form a saturated solution droplet containing about 13 moles H_2O/mole solute (#H_2O/Solute). Upon evaporation, the solution droplet becomes highly supersaturated until, finally, crystallization occurs at about 58 %RH, yielding an anhydrous particle.

At high supersaturations, decahydrate is no longer the most stable state. The relative stability between the anhydrous Na_2SO_4 and the decahydrate can be estimated from a consideration of the standard Gibb's free energy change, ΔG^o, of the system:

$$Na_2SO_4(c) + 10H_2O(g) = Na_2SO_4 \cdot 10H_2O(c) \ ,$$

so that,

$$\Delta G^o = \Delta G_f^o[Na_2SO_4 \cdot 10H_2O] - \Delta G_f^0[Na_2SO_4] - 10\Delta G_f^o[H_2O] = -RT \ln(1/p_1^{10}) \qquad (2)$$

Here, *c* and *g* in the parentheses refer to the crystalline state and gas phase, respectively. Taking the tabulated (Wagman et al. 1981) ΔG_f^o values -871.75, -303.59, and -54.635 kcal/mol for $Na_2SO_4 \cdot 10H_2O$(c), Na_2SO_4(c) and H_2O(g), respectively, we obtain a value of -21.81 kcal/mol for ΔG^o, which leads to 19.2 torr as the equilibrium partial pressure of water vapor, or 81 %RH at 25°C. It follows

that, instead of decahydrate, the anhydrous Na_2SO_4 becomes the most stable state below 81 %RH. Thus, as depicted by the dashed lines shown in Fig. 3, a solid anhydrous Na_2SO_4 particle would have transformed into a crystalline decahydrate particle at 81 %RH, which would then deliquesce at 93.6 %RH, to become a saturated solution droplet containing about 28 $\#H_2O$/Solute, according to solution thermodynamics (Goldberg, 1981). However, the observed hydration behavior of the particle, as shown in Fig. 3, is quite different from what is predicted from the bulk-phase thermodynamics.

The hydration behavior of a mixed-salt particle is more complicated in that partially dissolved states may be present. This is illustrated again in Figure 2 by the growth (filled circles) and evaporation (open circles) of a mixed-salt particle composed of 80% KCl and 20% NaCl by weight. The particle was observed to deliquesce at 72.5 %RH, followed by a region where excess KCl gradually dissolved in the solution as RH increased. The particle became a homogeneous solution droplet at 82 %RH. Upon evaporation, the solution droplet was observed to crystallize at about 61 %RH. Figure 4 shows the growth and evaporation of another mixed-salt particle composed of equal amounts of NaCl, Na_2SO_4, and $NaNO_3$. At 17.5°C, the particle was observed to deliquesce at 72 %RH (Tang and Munkelwitz, 1994). There was also a region following deliquescence where excess solids were gradually dissolving in the solution. At 74 %RH, this mixed-salt particle became a homogeneous solution droplet, which would then grow or evaporate as RH was increasing or decreasing, respectively, as shown in Figure 4. Upon evaporation, the particle was observed to persist as a metastable solution

droplet and finally crystallized at about 45 %RH. Thus, the general hydration characteristics are similar for multi-component aerosol particles.

Tang (1976) has considered the phase transformation and droplet growth of mixed-salt aerosols. The particle deliquescence is determined by the water activity of the eutonic point, E, in the solubility diagram, as shown in Figure 5 for the KCl-NaCl-H_2O system. Here, wt% NaCl is plotted vs. wt% KCl for ternary solutions containing the two salts as solutes and H_2O as the solvent. The solid curves, AE and BE, shown here for 25°C, are solubility curves constructed from data taken from Seidell and Linke (1965). Each point on the solubility curves determines the composition of a saturated solution in equilibrium with a specific water activity. Thus, point A represents the solubility of NaCl at concentration of 26.42 wt% and a_1 of 0.753, and point B is the solubility of KCl at 26.37 wt% and a_1 of 0.843. The solution is saturated with NaCl along the curve AE and with KCl along BE. The eutonic point, E, is the composition (KCl/NaCl = 11.14/20.42%) where both salts have reached their solubility limits in the solution at the given temperature. This is usually the composition at which the water activity is the lowest among all compositions (Kirgintsev and Trushnikova, 1968; Tang, 1976). It is, therefore, the composition of the solution droplet formed when a solid particle of any composition (for example, KCl/NaCl = 80/20%, as represented by point C) first deliquesces. Wexler and Seinfeld (1991) have shown theoretically that the RHD of one electrolyte is lowered by the addition of a second electrolyte, essentially explaining why RHD of a mixed-salt particle is lower than that of either single-salt particles.

Equilibrium Droplet Size and Water Activity

The equilibrium between an aqueous salt solution droplet and water vapor in humid air at constant temperature and relative humidity has been considered by many investigators since the earlier work of Koehler (1936). A thorough account of the thermodynamics of droplet-vapor equilibrium can be found in books by Dufour and Defay (1963) and by Pruppacher and Klett (1978). For a solution droplet containing nonvolatile solutes, the equation,

$$\ln \frac{p_1}{p_1^o} = \ln \gamma_1 y_1 + \frac{2\upsilon_1 \sigma}{RTr} \qquad (3)$$

is quite general and applies to both single and multicomponent systems, provided that the solution properties are determined for the system under consideration (Tang, 1976; 1980). Equation (3) relates the equilibrium radius r of a droplet of composition y_1 (mole fraction) to RH, namely, $\%RH = 100p_1/p_1^\circ$, and to the solution properties such as the activity coefficient γ_1, partial molar volume υ_1, and surface tension σ. Here, the subscript 1 refers to water as the solvent. p_1 is the partial pressure and p_1° the saturation vapor pressure of water at temperature T °K. R is the gas constant. For a droplet of 0.1 μm in diameter, the contribution of the second term on the right-hand side of Equation (3) is about 2%. Consequently, for larger droplets, the droplet composition agrees closely with that of a bulk solution in equilibrium with its water vapor at given T, and the water activity of the solution droplet is simply:

$$a_1 = \gamma_1 y_1 = \frac{p_1}{p_1^o} = \frac{\%RH}{100} \qquad (4)$$

The change in particle size at a given relative humidity can readily be deduced from a material balance on salt content before and after droplet growth to its equilibrium size. The following equation is obtained:

$$\frac{d}{d_o} = \left(\frac{100\rho_o}{x\rho}\right)^{1/3} \qquad (5)$$

Here, d and ρ are, respectively, the diameter and density of a droplet containing $x\%$ by weight of total salts. Again, the subscript, o, refers to the dry salt particle. It follows that, in order to calculate droplet growth as a function of RH, it is essential to have water activity and density data as a function of droplet composition.

The simplest measurements that can be made with the single-particle levitation technique are water activities of electrolyte solutions over a large concentration range, especially at high supersaturations that could not have been done with bulk solutions. For highly hygroscopic inorganic salts such as NH_4HSO_4, $NaHSO_4$, and $NaNO_3$, the solution droplets may persist in the liquid form to such a degree that one solvent molecule is shared by 5 or 6 solute molecules (Tang and Munkelwitz, 1994a). Such data are not only required in modelling the hydration behavior of atmospheric aerosols, but also crucial to testing and furthering the development of solution theories for high concentrations and multicomponent

systems. Indeed, some efforts have begun to modify and extend Pitzer's semi-empirical thermodynamic model for relativly dilute electrolyte solutions to high concentrations (Clegg and Pitzer, 1992; Clegg et al., 1992; Clegg and Brimblecombe, 1995).

$(NH_4)_2SO_4$ is one of the most important constituents of the ambient aerosol. A large effort has been made to obtain thermodynamic and optical data for modelling computations. Thus, Richardson and Spann (1984) have made water activity measurements at room temperature with $(NH_4)_2SO_4$ solution droplets levitated in a chamber which can be evacuated and back filled with water vapor. Cohen et al. (1987a), have employed an electrodynamic balance placed in a continuously flowing gas stream at ambient pressures and made water activity measurements for a number of electrolytes including $(NH_4)_2SO_4$. The two sets of data show some discrepancies, which amount to 0.04-0.05 in water activities or 5-6 wt% at high concentrations. Chan et al. (1992) have repeated the measurements in a spherical void electrodynamic levitator (SVEL) and obtained results consistent with those of Cohen et al. The SVEL is a variation of the electrodynamic balance with the inner surfaces of the electrodes designed to form a spherical void (Arnold and Folan, 1987). Tang and Munkelwitz (1994a) have also made extensive measurements in their apparatus, which is closer in design to that of Richardson and Spann but better thermostatted. Their results, together with those of previous studies, are shown in Figure 6. It appears that, although the agreement among all data sets is acceptable for aerosol growth computations, there is a need for more intercomparison studies to reduce the variability before the method can become

standardized for precise thermodynamic measurements. The discrepancies could be due to experimental uncertainties in balancing the particle at the null point, adverse effects of thermal convection in the cell, and unavoidable measurement errors in humidity and temperature.

Because of space limitations, as well as the specific purpose of this review, water activity and density data are given only for a few selected inorganic salt systems, most of which are of atmospheric interest. Both water activity and density are expressed in the form of a polynomial in x, the solute wt%, namely,

$$a_1 = 1 + \sum C_i x^i \tag{6}$$

and

$$\rho = 0.9971 + \sum A_i x^i \tag{7}$$

where the polynomial coefficients, C_i and A_i, are given in Table I.

Data for mixed-salt solutions are very limited. Tang et al. (1978; 1981) measured the water activity of bulk solutions of $(NH_4)_2SO_4/NH_4HSO_4$ (molar ratio 1/1) and $(NH_4)_2SO_4/NH_4NO_3$ (3/1; 1/2). Spann and Richardson (1985) measured the water activity of $(NH_4)_2SO_4/NH_4HSO_4$ ($1.5 \leq [NH_4^+]/[SO_4^=] \leq 2$) solution droplets, using the electrodynamic balance. Cohen et al. (1987b) used the electrodynamic balance to meseaure the water avtivity of mixed-electrolyte solution droplets containing NaCl/KCl, NaCl/KBr, or $NaCl/(NH_4)_2SO_4$. Chan et al. (1992) used the SVEL to measure the water activity of solution droplets containing various compositions of $(NH_4)_2SO_4/NH_4NO_3$. Recently, Kim et al. (1994) again used the

SVEL to measure the water activity of solution droplets for the $(NH_4)_2SO_4/H_2SO_4$ system. All investigators seem to agree that the simple empirical relationship, known as the ZSR relation (Zdanovskii, 1936; Stokes and Robinson, 1966), is capable of predicting with satisfaction the water activity of mixed-salt solutions up to high concentrations, although other more elaborate methods may perform better at low concentrations.

For a semi-ideal ternary aqueous solution containing two electrolytes (designated 2 and 3) at a total molality $m = m_2 + m_3$, the ZSR relation,

$$\frac{1}{m} = \frac{y_2}{m_{02}} + \frac{y_3}{m_{03}} \tag{8}$$

holds when the solution is in isopiestic equilibrium with the binary solutions of the individual electrolyte at respective molalities m_{02} and m_{03}. Here, $y_2 = m_2/m$ and $y_3 = m_3/m$. Semi-ideality refers to the case where the two solutes may interact with the solvent but not with each other. It is also conceivable that a solution behaves semi-ideally when the solute-solute interactions are present but cancelling each other. Systems showing departure from semi-ideality are common (Sanster and lenzi, 1974). For such systems, a third term, by_2y_3, may be added to the right-hand side of Eq. (8), where b is an empirically determined parameter for each system.

Particle Deliquescence

As discussed earlier, for single-salt particles larger than 0.1 μm, the deliquescence point corresponds to the saturation point of the bulk solution. Thus, %RHD for a single-salt aerosol particle is, in principle, equal to $100a_1^*$, where a_1^*

is the water activity of the saturated electrolyte solution. In Table II, the observed %RHD of some inorganic salt particles are compared with predictions from bulk solution data, which are available in the literature (e.g., West and Hull, 1933; Robinson and Stokes, 1970). Note that, within experimental uncertainties, the comparison is resonably good only for those inorganic salts whose stable crystalline phase in equilibrium with the saturated solution is identical to the observed particle phase.

For a ternary system consisting of two salts as solutes and water as solvent, it is possible to compute the water activity at the eutonic point using the ZSR method. Other estimation methods such as those by Meissner and Kusik (1972), Bromly (1973), and Pitzer (1973) are also available in the literature. Stelson and Seinfeld (1982) used the M-K method to calculate the water activities for the NH_4NO_3- $(NH_4)_2SO_4$- H_2O system and found a good agreement between the theoretical predictions and the experimental measurements of Tang et al. (1981). Koloutsou-Vakakis and Rood (1994) also presented a salient description of a thermodynamic model for predicting RHD for the $(NH_4)_2SO_4$-Na_2SO_4-H_2O system. They compared their %RHD predictions with field measurements by the temperature and humidity controlled nephelnometry, assuming the aerosol sample to be internally mixed.

Table III shows the comparison of the predicted %RHD by the M-K and ZSR methods with experimental measurements for a number of mixed-salt particles. It is shown that for simple mixed-salt systems, where no crystalline hydrates or double salts are present in the solid phases, the predictions are in good agreement

with the measurements. However, for more complicated systems such as the Na_2SO_4-$(NH_4)_2SO_4$ and the Na_2SO_4-$NaNO_3$ solutions, where the eutonic composition is in equilibrium with a double salt, the predicted %RHD is somewhat off. Also note that, since in an aerosol particle the solid phase may not be what is expected from the bulk solution, the observed %RHD may also be different from what is predected on the basis of the bulk-solution eutonic composition.

Klaue and Dannecker (1993; 1994) investigated the deliquescence properties of the double salts $2NH_4NO_3 \bullet (NH_4)_2SO_4$ (2:1) and $3NH_4NO_3 \bullet (NH_4)_2SO_4$ (3:1), using a humidity controlled x-ray diffractometer to observe changes in the crystalline phase. They concluded that %RHD for 2:1 was 68 %RH, instead of 56.4 %RH as reported by Tang (1980), who made the measurement in a continuous-flow aerosol apparatus. Subsequently, Tang et al. (1981) reported water activity measurements for mixed-salt solutions of NH_4NO_3-$(NH_4)_2SO_4$ and showed that the water activity at the eutonic composition was 0.66, clearly indicating that the earlier measurement was too low. The measurement error could have resulted from water adsoption on aerosol particles due to the presence of NH_4NO_3, which obscured the deliquecsence point, just as what might have happened in the case of pure NH_4NO_3 aerosol particles, using the continuous-flow method.

The temperature and composition dependence of the deliquescence humidity has been investigated by Tang and Munkelwitz (1993; 1994b). Consider, for example, a solid KCl particle surrounded by humid air at a temperature T. At its

deliquescence humidity corresponding to a water vapor partial pressure of p_1 atm, the particle transforms into a droplet by condensing, on a molar basis, one mole of water vapor, $H_2O(g)$, onto n moles of crystalline $KCl(c)$ to form a saturated aqueous solution of molality m_S. Assume again the diameter of the droplet to be larger than 0.1 μm so that the Kelvin effect due to surface tension can be ignored. The vapor-liquid equilibrium can be expressed by the following reactions:

$$H_2O(g) = H_2O(l) \tag{9}$$

$$H_2O(l) + n\,KCl(c) = KCl(aq,\ m_S) \tag{10}$$

Here, the symbols in the parentheses have the following meanings: g denotes vapor, l liquid, c crystalline, aq aqueous solution. The heat that is released in Reaction (9) is the heat of condensation of water vapor, which is equal to its heat of vaporization, $-\Delta H_V$. The heat that is absorbed in Reaction (10) is the integral heat of solution, ΔH_S, which may be calculated from the heats of formation tabulated in standard thermodynamic tables (Wagman *et al.*,1966). The overall heat involved in the process is the sum of the two heats:

$$\Delta H = n\,\Delta H_S - \Delta H_V \tag{11}$$

Thus, applying the Clausius-Clapeyron equation to the phase transformation, we have

$$\frac{d\ln p_1}{dT} = -\frac{\Delta H}{RT^2} = \frac{\Delta H_V}{RT^2} - \frac{n\,\Delta H_S}{RT^2} \tag{12}$$

Since by definition,

$$\frac{d\ln p_1^0}{dT} = \frac{\Delta H_V}{RT^2} \tag{13}$$

it follows that, by combining Eqs. (4), (12) and (13), we obtain

$$\frac{d\ln a_1}{dT} = -\frac{n\,\Delta H_S}{RT^2} \tag{14}$$

Here, n is the solubility in moles of solute per mole of water, which can be found either in International Critical Tables (West and Hull, 1933) or in the compilation by Seidell and Linke (1965). For the convenience of integrating Eq. (14), n is expressed as a polynomial in T

$$n = A + BT + CT^2 \tag{15}$$

Upon substituting n from Eq. (15) into (14), rearranging and integrating the resulting equation from a reference temperature, T^*, we obtain

$$\ln\frac{\%RHD(T)}{\%RHD(T^*)} = \frac{\Delta H_S}{R}\left[A\left(\frac{1}{T}-\frac{1}{T^*}\right) - B\ln\frac{T}{T^*} - C(T-T^*)\right] \tag{16}$$

Since for most electrolyte solutions the thermodynamic properties at 25°C are well documented, 298.2 °K is a convenient choice for T^*.

The derivation of Eq. (16) for a single-salt particle is straightforward. Edger and Swan (1922), in considering the vapor pressure of saturated aqueous solutions, used the Van't Hoff equation relating the solubility to the integral heat of solution and obtained an equation essentially showing that $\ln a_w$ is a linear function of n over a limited temperature increment. Recently, Wexler and Seinfeld (1991) derived a similar but simplified equation by assuming both

constant latent heat and constant saturation molality over a small temperature change. Thus, the derivation of Eq. (16) here is more rigorous, assuming only that the integral heat of solution is constant.

Eq. (16) shows that the effect of temperature on %RHD is predominantly governed by the sign and magnitude of the integral heat of solution. In Table IV, the parameters required for computing %RHD by Eq.(16) are given for a few inorganic salts of atmospheric interest. Figure 7 shows a comparison of %RHD between the bulk solution data (open symbols) and the single-particle measurements (filled circles) for the $NaNO_3$-H_2O system. A comparison is also shown between calculations by Eq. (16) (solid curve) and by a simpler formula (dashed curve) given by Wexler and Seinfeld (1991). It is apparent that, while in general the agreement between measurements and theory is good, the single-particle data show less scatter than the bulk-solution data and agree better with theoretical predictions. The two theoretical models also agree with each other in the limited temperature range 10-30°C, but start to show some departure at other temperatures as a result of different assumptions used in the solubility data.

For mixed-salt systems, particle deliquescence is determined by the water activity at the eutonic point. Consider, therefore, the deliquescence of a mixed-salt particle at the eutonic composition represented by n_2 moles of NaCl, n_3 moles of KCl and one mole of H_2O:

$$H_2O(l) + n_2NaCl(c) + n_3KCl(c) = Solution \qquad (17)$$

Because of a lack of experimental data for multicomponent systems, the heat that

is absorbed in Reaction (17) can only be estimated from the respective integral heats of solution for the binary solutions, NaCl-H_2O and KCl-H_2O, namely,

$$\Delta H_S = n_2 \Delta H_{S2} + n_3 \Delta H_{S3} - \Delta H_1 \tag{18}$$

Here, the subscript 1 refers to the solvent and the other numbers refer to the solutes. The last term in Eq. (18) accounts for the fact that ΔH_1, the differential heat of solution due to the solvent, has been included in each of the two integral heats of solution and, therefore, should be subtracted once from the total heat of solution. This is usually a small correction term and may be neglected in most cases.

The solubilities, n_2 and n_3 , may be obtained from the eutonic composition and expressed as a function of temperature like Equation (15). Sometimes, polynomials higher than the second order may be needed. Substituting Eq. (18) into (14), rearranging, and integrating lead to the final equation (Tang and Munkelwitz, 1993):

$$\ln \frac{\%RHD(T)}{\%RHD(T^*)} = \frac{\Delta H_{S2}}{R}\left[A_2\left(\frac{1}{T}-\frac{1}{T^*}\right) - B_2 \ln\frac{T}{T^*} - C_2(T-T^*)\right] + \frac{\Delta H_{S3}}{R}\left[A_3\left(\frac{1}{T}-\frac{1}{T^*}\right) - B_3 \ln\frac{T}{T^*} - C_3(T-T^*)\right] - \frac{\Delta H_1}{R}\left(\frac{1}{T}-\frac{1}{T^*}\right) \tag{19}$$

Eq. (19) was derived strictly for the case of simple two-component mixtures forming a single eutonic composition in saturated solutions. Further work is needed for more complex aerosol systems.

Figures 8 and 9 show, respectively, the results obtained for aerosol particles containing various compositions of KCl-NaCl and $NaNO_3$-NaCl. The two lines

shown for the single-salt particles are computed from theory, using tabulated parameters given in Table IV. The corresponding line for mixed-salt particles is computed from Eq. (19) and pertinent data in Table V. It is clear that the agreement between theory and experiment is good. The slight but noticeable departure at either end of the theoretical line may be due to our assumption of additive heats of solution made in Eq. (18). Since there is no experimental heat of solution data available for the multi-component systems of atmospheric interest, Eq. (19) derived on the basis of additive properties may still be used to provide a reasonable estimate in any ambient aerosol modelling studies, at least in a limited temperature region. It is also worthwhile to point out that, for salt mixtures having simple solubility properties, the deliquescence humidity is governed only by the water activity at the eutonic composition and is thus independent of the initial dry-salt composition. The temperature dependence of the mixed-salt particle usually more or less follows the direction of the component salt whose eutonic solubility is the higher of the two.

As discussed earlier, no simple mathematical analysis is yet possible at the present time for mixed-salt particles containing more than two deliquescent salts. The deliquescence properties of the three-salt system, $NaCl$-Na_2SO_4-$NaNO_3$, whose growth curve is shown in Figure 4, was studied in the limited temperature range 12-33°C. The results shown in Figure 10 indicate that, within the experimental error, the deliquescence humidity may be considered constant at 71.8±0.5%. A least-squares line drawn through the data points shows only very slightly, if any, temperature dependent. Since ambient aerosols are likely multi-component

systems composed of more than two inorganic salts, further work to elucidate the hygroscopic properties of these complex aerosols is needed in order to predict their transport and light-scattering behavior in a humid environment.

Solute Nucleation and Droplet Efflorescence

The persistence of a solution drop during evaporation to high degrees of supersaturation with respect to the solute is typical of suspended hygroscopic aerosol particles, which are free of the presence of foreign substrates. While the droplet is in equilibrium with the surrounding water vapor, it is metastable with respect to the solid-phase solute. Therefore, solute nucleation is expected: the higher the degree of supersaturation the larger the nucleation rate (Walton, 1967). According to the classical nucleation theory, the net rate of embryo formation, J, per uint volume per unit time is given by:

$$J = K \exp(-\Delta G_c / kT) \tag{20}$$

where ΔG_c is the maximum free-energy barrier to transition to the more stable phase and k the Boltsman constant. K, an undetermined kinetic factor, is either estimated from the binary collision frequency according to the reation rate theory (Turnbull and Fisher, 1949) or expressed by some complex formula derived from various theories as discussed by Tamara et al. (1993). Theoretical estimates of its value range from 10^{24} to 10^{36} cm^{-3} sec^{-1}. An intermediate value that has been commonly used is 10^{30}. For a given rate of critical nucleus formation, J, the expected induction time, t_i, before a nucleation event happens in a droplet of volume, V_d, is given by (Cohen et al., 1987c):

$$t_i = \frac{1}{V_d J} \tag{21}$$

Substituting Eq. (21) into Eq. (20) and rearranging, we have

$$\Delta G_c = kT \ln (V_d t_i K) \tag{22}$$

Assume that the nucleation embryos are crystallites formed by density fluctuations in the supersaturated solution droplet. The free-energy barrier to nucleation of a given sized crystalline embryo is

$$\Delta G = A\sigma + V\Delta G_v \tag{23}$$

where A and V are, respectively, the total interfacial area and volume of the embryo, σ is the average interfacial free energy based on A, and ΔG_V is the excess free energy per unit volume of the embryo over that of the solution. For simplicity, the embryo is usually assumed to be spherical in shape so that A and V may be expressed in term of its radius, r. Other shapes consistent with the unit cells specific to given crystalline habits have also been considered, using an approprietely defined characteristic length (Enüstün and Turkevich, 1960; Tang and Munkelwitz, 1984; Cohen et al., 1987c).

If the solute in the saturated solution is chosen as the referenc state and the definition of the solute mean activities is invoked, then, ΔG_V is given by

$$\Delta G_v = -\frac{\nu \rho_o RT}{M} \ln \frac{a_\pm}{a_\pm^*} \tag{24}$$

where $a_\pm$ and $a_\pm^*$ are, respectivly, the solute mean activities in the supersaturated

and in the saturated solutions. M is the solute molecular weight, ρ_o is the density of the crystalline phase, and ν is the number of ions produced by the dissociation of a salt molecule.

The critical size of the embryo corresponding to the maximum free-energy barrier is obtained, in the case of a spherical embryo, by lettting $(\partial \Delta G/\partial r) = 0$. Hence (Tang and Munkelwitz, 1984),

$$r_c = -\frac{2\sigma}{\Delta G_v} \tag{25}$$

and, consequently,

$$\sigma^3 = \frac{3kT \ln(V_d t_i K)}{16\pi}\left[\frac{\nu \rho_o RT}{M} \ln S_{\pm}\right]^2 \tag{26}$$

where $S_{\pm}$ is the critical supersaturation at the onset of crystallization and is given by the ratio, $a_{\pm}/a_{\pm}^*$. Using the Gibbs-Duhem equation, ln $S_{\pm}$ may be calculated from the water activity measurement according to the following equation (Stokes and Robinson, 1970):

$$\ln S_{\pm} = \int_{a_1^*}^{a_1} \frac{55.51}{\nu m} d\ln a_1 \tag{27}$$

Here, $ln a_1$ is usually expressed as a polynomial in solute molality for the convenience of carrying out the integration.

In droplet crystallization experiments, $S_{\pm}$ can be measured with much higher precision than what would be possible in bulk solution studies. Thus, the

uncertainties in σ determination by the single-particle levitation experiment lie largely in estimating the product $(V_d\, t_i\, K)$. Taking a typical droplet of 15 μm in diameter, an induction time about one sec, and 10^{30} for K, the estimate of $\ln(V_d t_i K)$ is about 49, a representative value for ionic solution droplets. A change in the product by two orders of magnitude results in about 3% change in the value of σ, whereas a 15% change in S would lead to about 7% change in σ.

In Table VI, the estimated interfacial energy, σ, critical embryo size, r_c, and number of molecles, N, in the spherical embryo are given for some common inorganic salts. The calculation is based on the solute concentration in molality, m, and supersaturation, S, measured at the onset of solute nucleation in droplets. It is worthwhile to note that, although for each system there are discrepancies in the observed critical supersaturations, the estimated embryo properties show reasonable agreement. In addition, the nucleation embryo properties for $NaNO_3$, a highly hygroscopic salt, do not vary much, despite the fact that the critical solute concentration may span a wide range from 78 to 380 m. The invariance appears to give credence to the embryo properties determined from studies of homogeneous nucleation in suspended aqueous solution droplets.

Acknowledgment. The author is indebted to his colleague, Harry. R. Munkelwitz, who designed and constructed the single-particle levitation apparatus and performed the experiments reported through the years. This research was performed under the auspices of the U.S. Department of Energy under Contract No. DE-AC02-76CH00016.

References

Arnold, S. and Folan, L. M. (1987) *Rev. Sci. Instr.* **58**, 1732

Bromley, L. A. (1973) *AIChE J.* **19**, 313

Chan, C. K., Flagan, R. C. and Seinfeld, J. H. (1992) *Atmos. Environ.* **26A**, 1661

Clegg, S. L. and Brimblecombe, P. (1995) *J. Aerosol Sci.* **26**, 19

Clegg, S. L. and Pitzer, K. S. (1992) *J. Phy. Chem.* **96**, 3513

Clegg, S. L., Pitzer, K. S. and Brimblecombe, P. (1992) *J. Phy. Chem.* **96**, 9470

Cohn, M. D., Flagan, R. C. and Seinfeld, J. H.(1987a) *J. Phys. Chem.* **91**, 4563

Cohn, M. D., Flagan, R. C. and Seinfeld, J. H.(1987b) *J. Phys. Chem.* **91**, 4575

Cohn, M. D., Flagan, R. C. and Seinfeld, J. H.(1987c) *J. Phys. Chem.* **91**, 4583

Covert, D. S., Charlson, R. J. amd Ahlquist, N. C. (1972) *J. Appl. Meteor.* **11**, 968

Davis, E. J. (1983) *Aerosol Sci. Technol.* **2**, 121

Davis, E. J. (1985) *Langmuir* **1**, 379

Davis, E. J. (1992) in Advances in Chemical Engineering, vol.**18**, Academic, San Diego

Dessens, H. (1949) *Q. J. R. Meteor. Soc.* **75**, 23

Dingemans, P. and Dijkgraaf, L. L. (1948) *Rec. Trav. Chim.* **67**, 231

Dufour, L. and Defay, R. (1963) Thermodynamic of Clouds, Academic, New York

Edger, G. and Swan, W. O. (1922) *J. Am. Chem. Soc.* 44, 570

Enustun, B. V. and Turkevich, J. (1960) *J. Am. Chem. Soc.* **82**, 4502

Frickel, R. B., Shaffer, R. E., and Stamatoff, J. B. (1978) Chambers for the Electrodynamic Containment of Charged Particles, U. S. Department of Commerce, National Technical Information Service, Report #AD/A056 236

Goldberg, R. N. (1981) *J. Phys. Chem. Ref. Data* **10**, 671

Junge, C. E. (1952) *Ann Met.* **5**, 1

Kim, Y. P., Pun, B. K.-L., Chan, C. K., Flagan, R. C. and Seinfeld, J. H. (1994) *Aerosol Sci. Technol.* **20**, 275

Kirgintsev, A. N. and Trushnikova, L. N. (1968) *Russ. J. Inorg. Chem.* **13**, 600

Klaue, B. and Dannecker, W. (1993) J. Aerosol Sci. 25, S189

Klaue, B. and Dannecker, W. (1994) J. Aerosol Sci. 25, S287

Koehler, H. (1936) *Trans. Farad. Soc.* **32**, 1152

Koloutsou-Vakakis, S. and Rood, M. J. (1994) *Tellus* **46B**, 1

La Mer, V. K. and Gruen, R. (1952) *Trans. Farad. Soc.* **48**, 410

Meissner, H. P. and Kusik, C. L. (1972) *AIChE J.* **18**, 294

Orr, C, Jr., Hurd, F. K. and Corbett, W. J. (1958) *J. Colloid Sci.* **13**, 472

Pitzer, K. S. (1973) *J. Phys. Chem.* **77**, 268

Pruppacher, H. R. and Klett, J. D. (1978) Microphysics of Cloud and Precipitation, D. Reidel, Dordrecht, Holland

Richardson, C. B. and Spann, J. F. (1984) *J. Aerosol Sci.* **15**, 563

Richardson, C. B. and Kurtz, C. A. (1984) *J. Am. Chem. Soc.* **106**, 6615

Robinson, R. A. and Stokes, R. H. (1970) Electrolyte Solutions, Butterworth, London

Rood, M. J., Shaw, M. A., Larson, T. V. and Covert, D. S. (1989) *Nature* **337**, 537

Sanster, J. and Lenzi, F. (1974) *Can. J. Chem. Eng.* **52**, 392

Seidell, A. and Linke, W. F. (1965) Solubilities of Inorganic and Metal Organic Compounds, 4th ed., Am. Chem. Soc., Washington, D.C.
Spann, J. F. and Richardson, C. B. (1985) *Atms. Environ.* **19**, 819
Stelson, A. W. and Seinfeld, J. H. (1982) *Atms. Environ.* **16**, 2507
Stokes, R. A. and Robinson, R. H. (1966) *J. Phys. Chem.* **70**, 2126
Straubel, H. (1956) *Z. Elektrochem.* **60**, 1033
Tamara, D., Snyder, T. D. and Richardson, C. B. (1993) *Langmuir* **9**, 347
Tang, I. N. (1976) *J. Aerosol Sci.* **7**, 361
Tang, I. N. (1980) In Generation of Aerosols, Willeke, K. Ed., Chapter 7, Ann Arbor Sci., Ann Arbor, Michigan
Tang, I. N. and Munkelwitz, H. R. (1977) *J. Aerosol Sci.* **8**, 321
Tang, I. N. and Munkelwitz, H. R. (1984) *J. Colloid Interface Sci.* **98**, 430
Tang, I. N. and Munkelwitz, H. R. (1991) *Aerosol Sci. Technol.* **15**, 201
Tang, I. N. and Munkelwitz, H. R. (1993) *Atms. Environ.* **27A**, 467-473
Tang, I. N. and Munkelwitz, H. R. (1994a) *J. Geophys. Res.* **99**, 18801
Tang, I. N. and Munkelwitz, H. R. (1994b) *J. Appl. Meteor.* **33**, 791
Tang, I. N., Munkelwitz, H. R. and Davis, J. G. (1978) *J Aerosol Sci.* **9**, 505
Tang, I. N., Munkelwitz, H. R. and Wang, N. (1986) *J. Colloid Interface Sci.* **14**, 409
Tang, I. N., Wong, W. T., and Munkelwitz, H. R. (1981) *Atms. Environ.* **15**, 2463
Tang, I. N., Fung, K. H., Imre, D. G., Munkelwitz, H. R. (1995) *Aerosol Sci. Technol.* in press
Turnbull, D. and Fisher, J. C. (1949) *J. Chem.Phys.* **17**, 71
Twomey, S. (1954) *J. Meteor.* **11**, 334
Wagman, D. D., Evans, W. H., Halow, I., Parker, V. B., Bailey, S. M. and Schumm, R. H. (1966) Selected Values of Chemical Thermodynamic Properties, National Bureau of Standards Technical Note 270, U.S. Department of Commerce, Washington, D.C.
Walton, A. G. (1967) The Formation and Properties of Precipitates, Interscience, New York
Wexler, A. S. and Seinfeld, J. H. (1991) *Atmos. Environ.* **25A**, 2731
West, C. J. and Hull C. (1933) International Critical Tables. McGraw-Hill, New York
Winkler, P. (1973) *J. Aerosol Sci.* **4**, 373
Winkler, P. and Junge, C. E. (1972) *J. Rech. Atm.* **6**, 617
Wueker, R. F., Shelton, H. and Langmuir, R. V. (1959) *J. Appl. Phys.* **30**, 342
Zdanovskii, A. B. (1936) *Trudy Solyanoi Laboratorii Akad. Nauk SSSR*, No. **6**

Table I. Summary of Polynomial Coefficients for Water Activities and Densities

	$(NH_4)_2SO_4$	NH_4HSO_4	$(NH_4)_3H(SO_4)_2$	Na_2SO_4		$NaHSO_4$	$NaNO_3$	NaCl
x (%)	0 - 78	0 - 97	0 - 78	0 - 40	40 -67*	0 - 95	0 - 98	0 - 48
C_1	-2.715(-3)	-3.05(-3)	-2.42(-3)	-3.55(-3)	-1.99(-2)	-4.98(-3)	-5.52(-3)	-6.366(-3)
C_2	3.113(-5)	-2.94(-5)	-4.615(-5)	9.63(-5)	-1.92(-5)	3.77(-6)	1.286(-4)	8.624(-5)
C_3	-2.336(-6)	-4.43(-7)	-2.83(-7)	-2.97(-6)	1.47(-6)	-6.32(-7)	-3.496(-6)	-1.158(-5)
C_4	1.412(-8)						1.843(-8)	1.518(-5)
A_1	5.92(-3)	5.87(-3)	5.66(-3)	8.871(-3)		7.56(-3)	6.512(-3)	7.41(-3)
A_2	-5.036(-6)	-1.89(-6)	2.96(-6)	3.195(-5)		2.36(-5)	3.025(-5)	-3.741(-5)
A_3	1.024(-8)	1.763(-7)	6.68(-8)	2.28(-7)		2.33(-7)	1.437(-7)	2.252(-6)
A_4								-2.06(-8)

* For this concentration range, $a_w = 1.557 + \sum C_i x_i$

Table II. Predicted and Observed %RHD for Some Pure-Salt Particles

Salt	Solution Phase	Particle Phase	Pred.%RHD	Obs. %RHD
NaCl	anhy.	anhy.	75.3	75.3±0.1
KCl	anhy.	anhy.	84.3	84.2±0.3
$(NH_4)_2SO_4$	anhy.	anhy.	80.0	79.9±0.5
NH_4HSO_4	anhy.	anhy.	39.7	40.3±0.5
Na_2SO_4	decahydrate	anhy.	93.6	84.5±0.5
$NaNO_3$	anhy.	anhy.	73.8	74.1±0.5
NH_4NO_3	anhy.	anhy.	61.8	61.2±0.5
$Sr(NO_3)_2$	tetrahydrate	amorphous	85	69.1±0.5

Table III. Predicted and Observed %RHD for Some Mixed-Salt Particles

System	Eutonic Composition	Solution Phases	Obs. %RHD	Pred. %RHD	
				K-M Method	ZSR Method
KCl(A)	2.183	A + B	72.7±0.3	71.7	72.1
NaCl(B)	5.106				
$NaNO_3$(A)	6.905	A + B	68.0±0.4	65.7	67.1
NaCl(B)	4.161				
Na_2SO_4(A)	1.057	A·B·4H_2O +B	71.3±0.4	76.4	76.4
$(NH_4)_2SO_4$(B)	5.494				
Na_2SO_4(A)	0.708	A + B	74.2±0.3	75.5	74.7
NaCl(B)	5.530				
Na_2SO_4(A)	0.413	A·B·2H_2O +B	72.2±0.2	74.6	74.1
$NaNO_3$(B)	10.28				

Table IV. Thermodynamic and Solubility Data of Electrolyte Solutions

System	*%RHD*	ΔH_S (cal/mol)	*A*	*B*	*C*
$(NH_4)_2SO_4$	79.9±0.5	1510	0.1149	-4.489 (-4)	1.385 (-6)
Na_2SO_4	84.2±0.4	-2330	0.3754	-1.763 (-3)	2.424 (-6)
$NaNO_3$	74.3±0.4	3162	0.1868	-1.677 (-3)	5.714 (-6)
NH_4NO_3	61.8	3885	4.298	-3.623 (-2)	7.853 (-5)
KCl	84.2±0.3	3665	-0.2368	1.453 (-3)	-1.238 (-6)
NaCl	75.3±0.1	448	0.1805	-5.310 (-4)	9.965 (-7)

Table V. Thermodynamic and Solubility Data of Aqueous Mixed-Salt Solutions

System	*%RHD* at *T**	ΔH_{si} (cal/mol)	A_i	B_i	C_i	D_i
NaCl	72.7±0.3	448	2.618(-1)	-9.412(-4)	1.254(-6)	
KCl		3665	-6.701(-2)	1.394(-4)	7.225(-7)	
Na_2SO_4	72.2±0.2	-2330	-4.591	4.413(-2)	-1.407(-4)	1.489(-7)
$NaNO_3$		3162	6.134	-5.847(-2)	1.852(-4)	1.879(-7)
$(NH_4)_2SO_4$	71.3±0.4	1510	1.977(-2)	2.617(-4)		
Na_2SO_4		-2330	-2.187	2.343(-2)	-8.411(-5)	1.017(-7)
NaCl	68.0±0.4	448	5.957(-1)	-3.745(-3)	9.134(-6)	-8.173(-9)
$NaNO_3$		3162	4.532(-1)	-4.106(-3)	9.909(-6)	5.552(-10)
NaCl	74.2±0.3	448	-5.313(-1)	5.477(-3)	-1.631(-5)	1.689(-8)
Na_2SO_4		-2330	-4.584(-1)	5.000(-3)	-1.723(-5)	1.933(-8)

Table VI. Properties of Nucleation Embryos in Aqueous Salt Solutions

Salt	m(critical)	S(critical)	σ(ergs/cm^2)	r(critical)	N(# molecles)
NaCl	13.8 [a]	5.15 [a]	104	6.81	30
	13	5.23	103	6.84	30
KCl	12.3 [a]	3.64 [a]	70.4	8.26	38
	12.6 [b]	3.4 [b]	67.9	8.41	40
	12.5	2.91	62.0	8.81	46
$(NH_4)_2SO_4$	17.5 [a]	2.52 [a]	46.6	10.2	35
	30	3.05	52.8	9.55	29
Na_2SO_4	13.2 [a]	3.71 [a]	74.1	8.06	25
	14	2.7	61.6	8.83	33
$NaNO_3$	78	2.97	62.9	8.74	45
	380	3.45	68.5	8.38	39

Figure Captions

Figure 1. Schematic diagram of the single-particle levitation apparatus.

Figure 2. Growth and evaporation of KCl/NaCl particles in humid environment at 25°C.

Figure 3. Growth and evaporation of a Na_2SO_4 particle in humid environment at 25°C.

Figure 4. Growth and evaporation of a mixed-salt particle composed of NaCl, Na_2SO_4, and $NaNO_3$ in humin environment at 17.5°C.

Figure 5. Solubility diagram for the system KCl-NaCl-H_2O at 25°C.

Figure 6. Water activities of aqueous $(NH_4)_2SO_4$ solutions as 25°C.

Figure 7. Deliquescence humidities as a function of temperature for $NaNO_3$ particles.

Figure 8. Deliquescence humidities as a function of temperature for mixed KCl-NaCl particles.

Figure 9. Deliquescence humidities as a function of temperature for mixed Na_2SO_4- $NaNO_3$ particles.

Figure 10. Deliquescence humidities as a function of temperature for mixed Na_2SO_4- $NaNO_3$- NaCl particles.

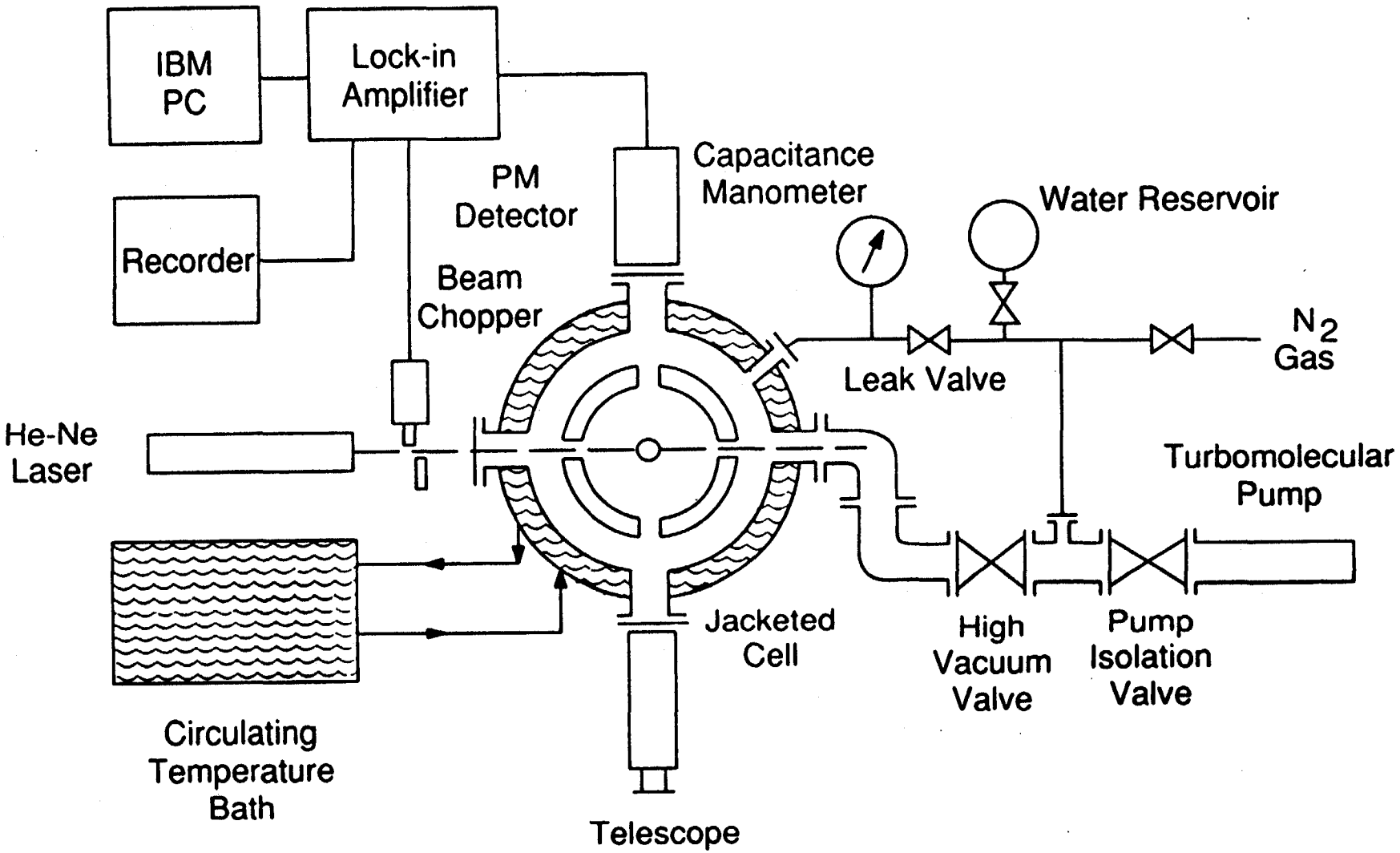
IBM PC
Lock-in Amplifier
Recorder
PM Detector
Capacitance Manometer
Water Reservoir
Beam Chopper
N_2 Gas
Leak Valve
He-Ne Laser
Turbomolecular Pump
Jacketed Cell
High Vacuum Valve
Pump Isolation Valve
Circulating Temperature Bath
Telescope

Figure 1

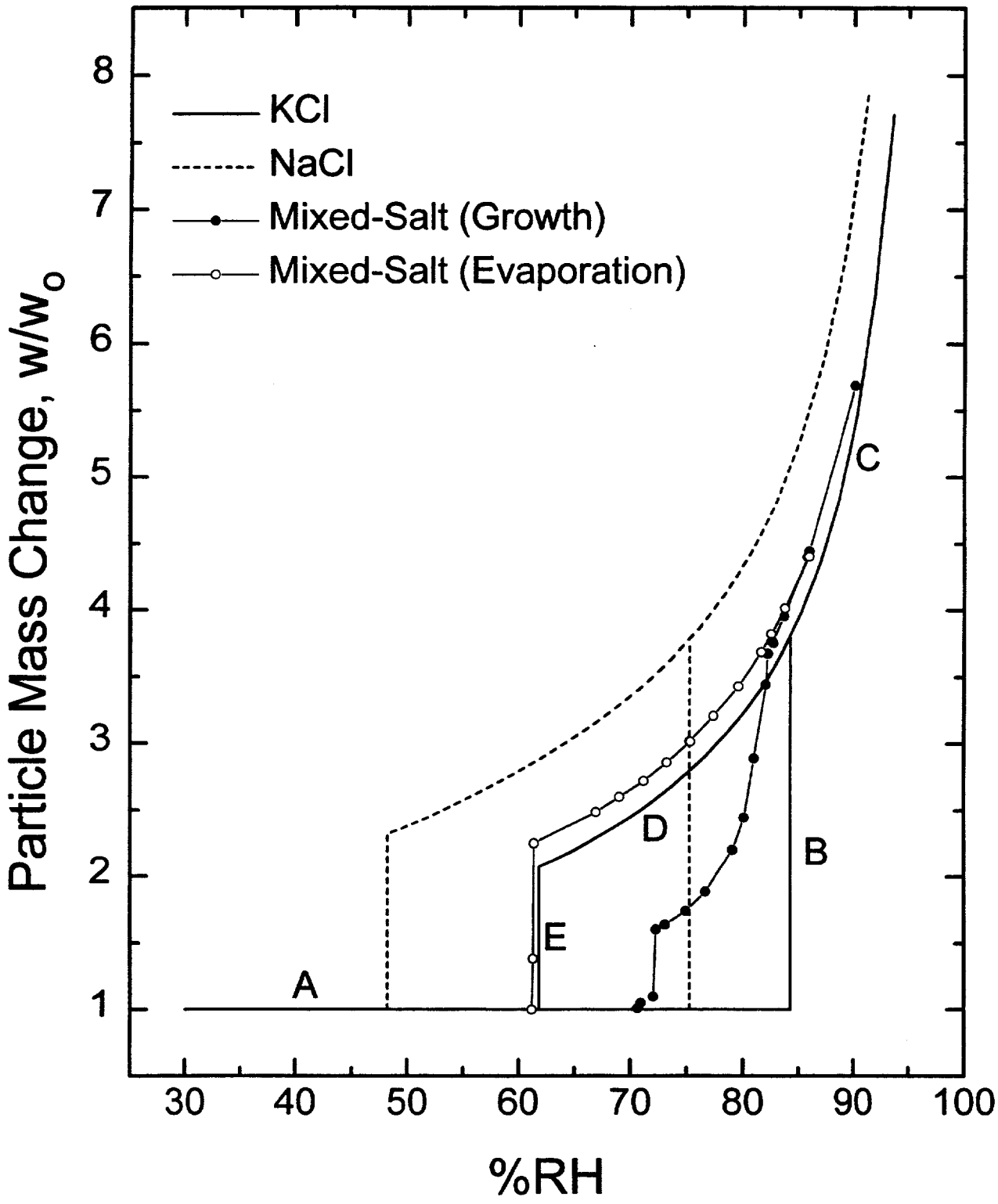
KCl
NaCl
Mixed-Salt (Growth)
Mixed-Salt (Evaporation)
Particle Mass Change, w/w$_o$
%RH
A
B
C
D
E
1
2
3
4
5
6
7
8
30
40
50
60
70
80
90
100

Figure 2

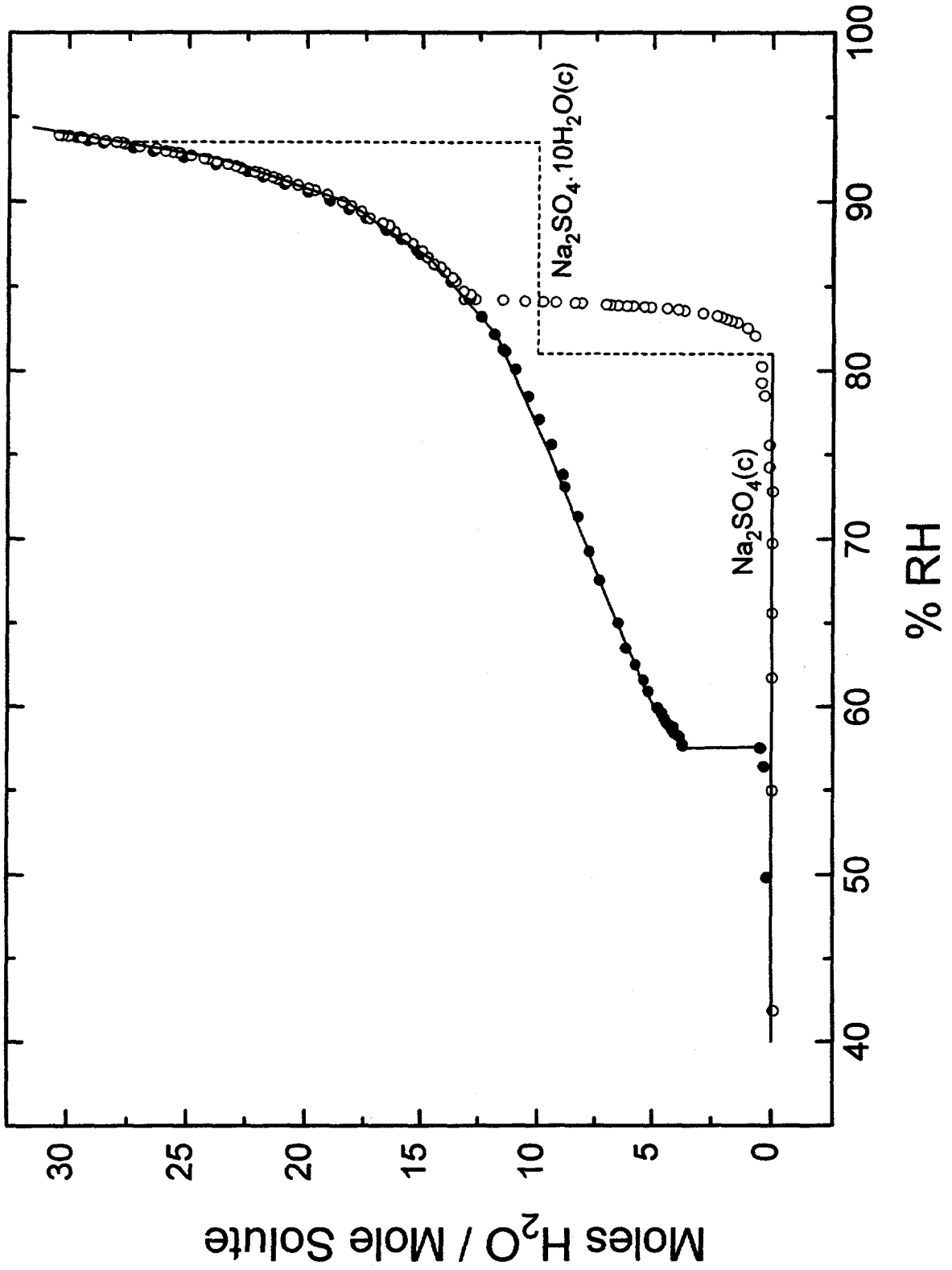
Moles H2O / Mole Solute
0
5
10
15
20
25
30
% RH
40
50
60
70
80
90
100
Na2SO4.10H2O(c)
Na2SO4(c)

Figure 3

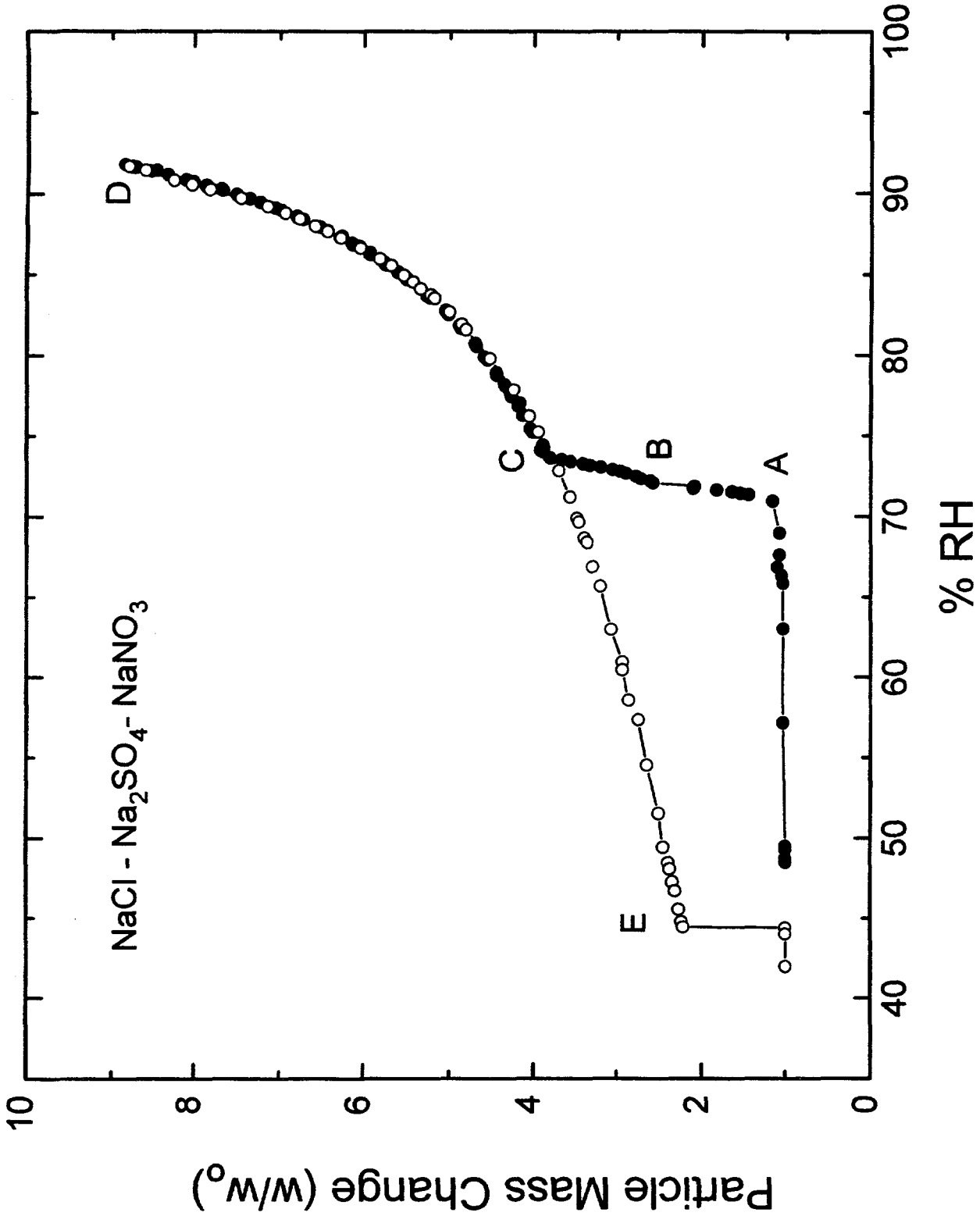
Particle Mass Change (w/w$_o$)
% RH
NaCl - Na_2SO_4- $NaNO_3$
A
B
C
D
E
0
2
4
6
8
10
40
50
60
70
80
90
100

Figure 4

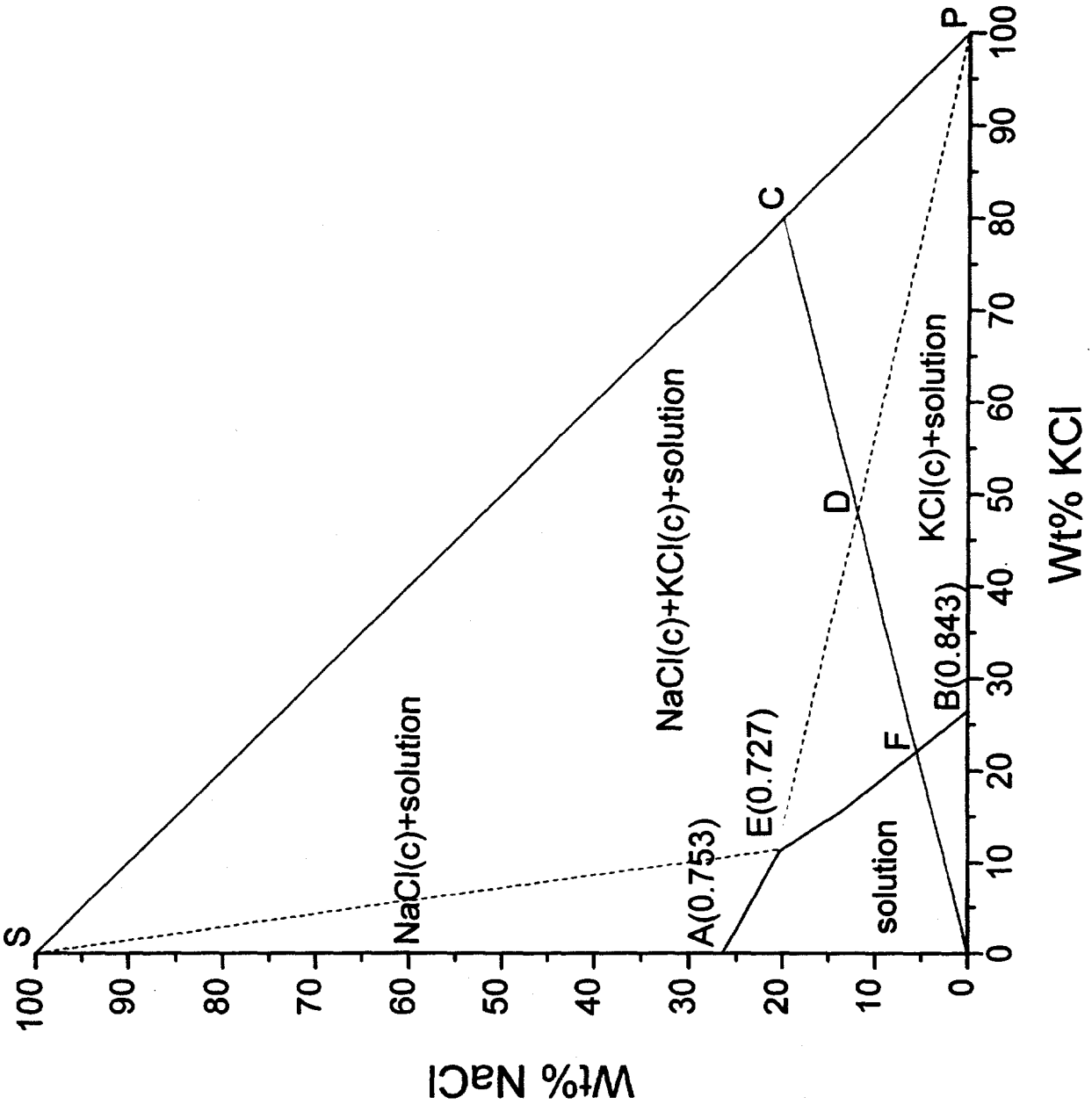
S
P
C
D
F
E(0.727)
A(0.753)
B(0.843)
NaCl(c)+solution
NaCl(c)+KCl(c)+solution
KCl(c)+solution
solution
Wt% NaCl
Wt% KCl
100
90
80
70
60
50
40
30
20
10
0
0
10
20
30
40
50
60
70
80
90
100

Figure 5

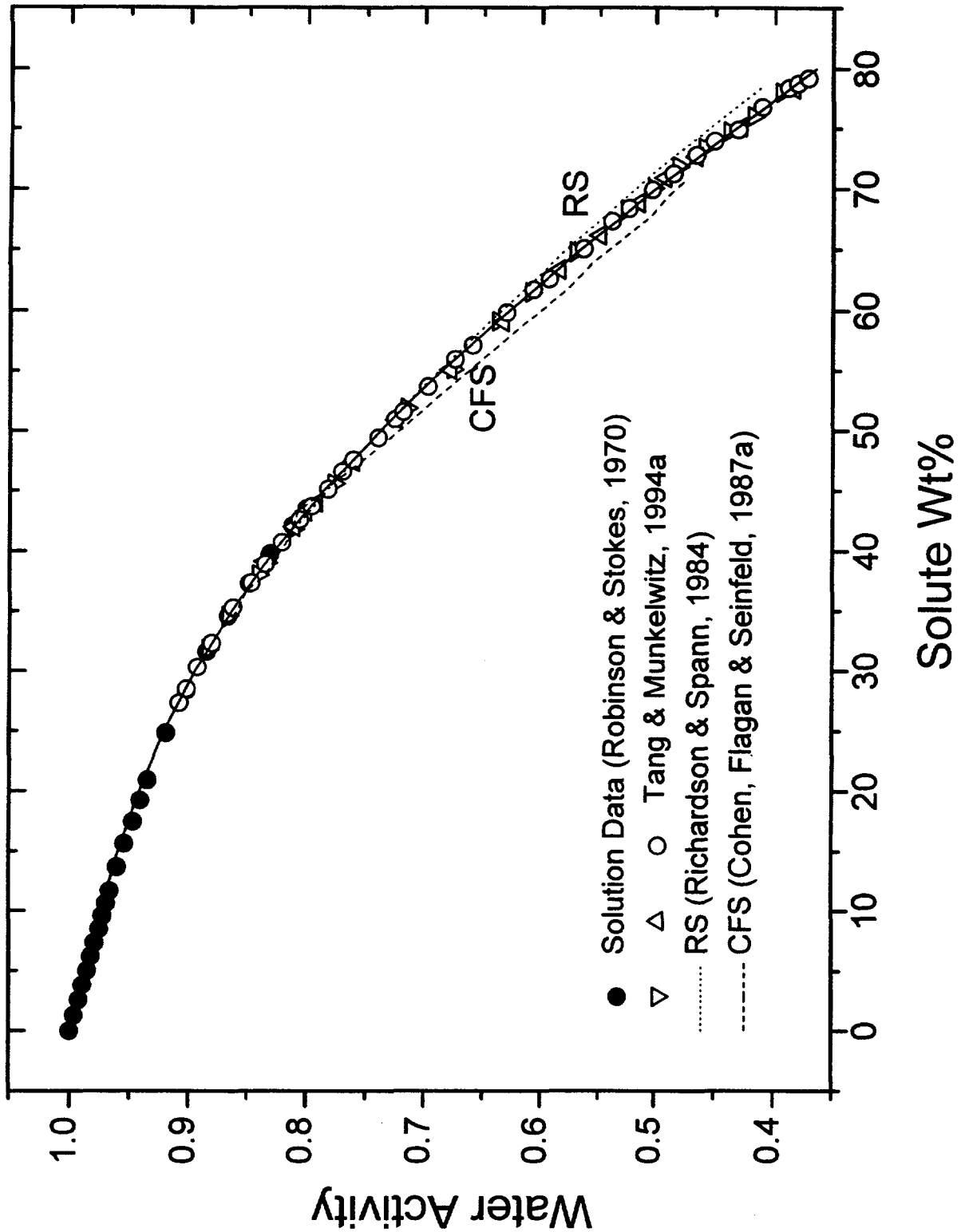
Water Activity
1.0
0.9
0.8
0.7
0.6
0.5
0.4
Solute Wt%
0
10
20
30
40
50
60
70
80
CFS
RS
Solution Data (Robinson & Stokes, 1970)
Tang & Munkelwitz, 1994a
RS (Richardson & Spann, 1984)
CFS (Cohen, Flagan & Seinfeld, 1987a)

Figure 6

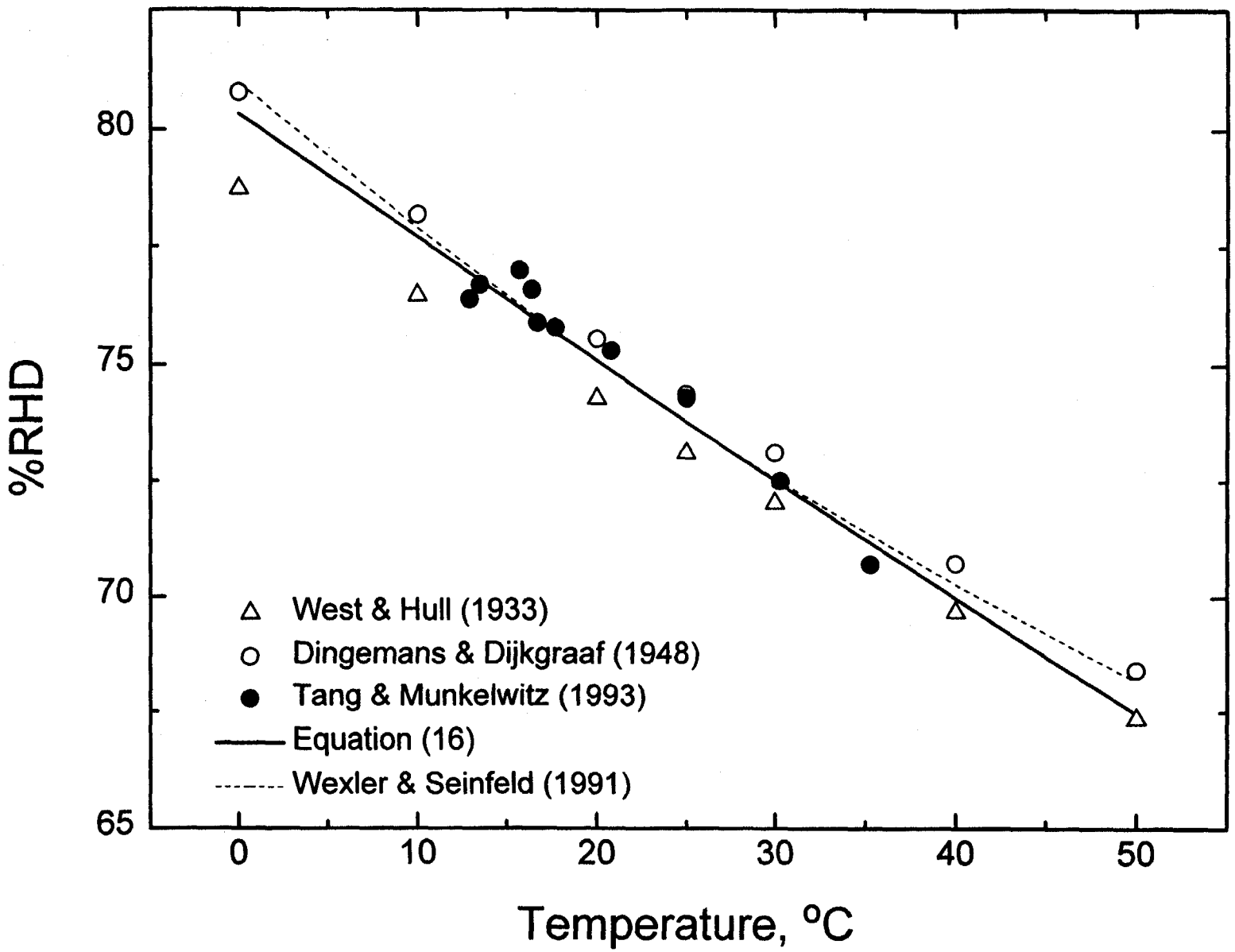
%RHD
80
75
70
65
0
10
20
30
40
50
Temperature, °C
West & Hull (1933)
Dingemans & Dijkgraaf (1948)
Tang & Munkelwitz (1993)
Equation (16)
Wexler & Seinfeld (1991)

Figure 7

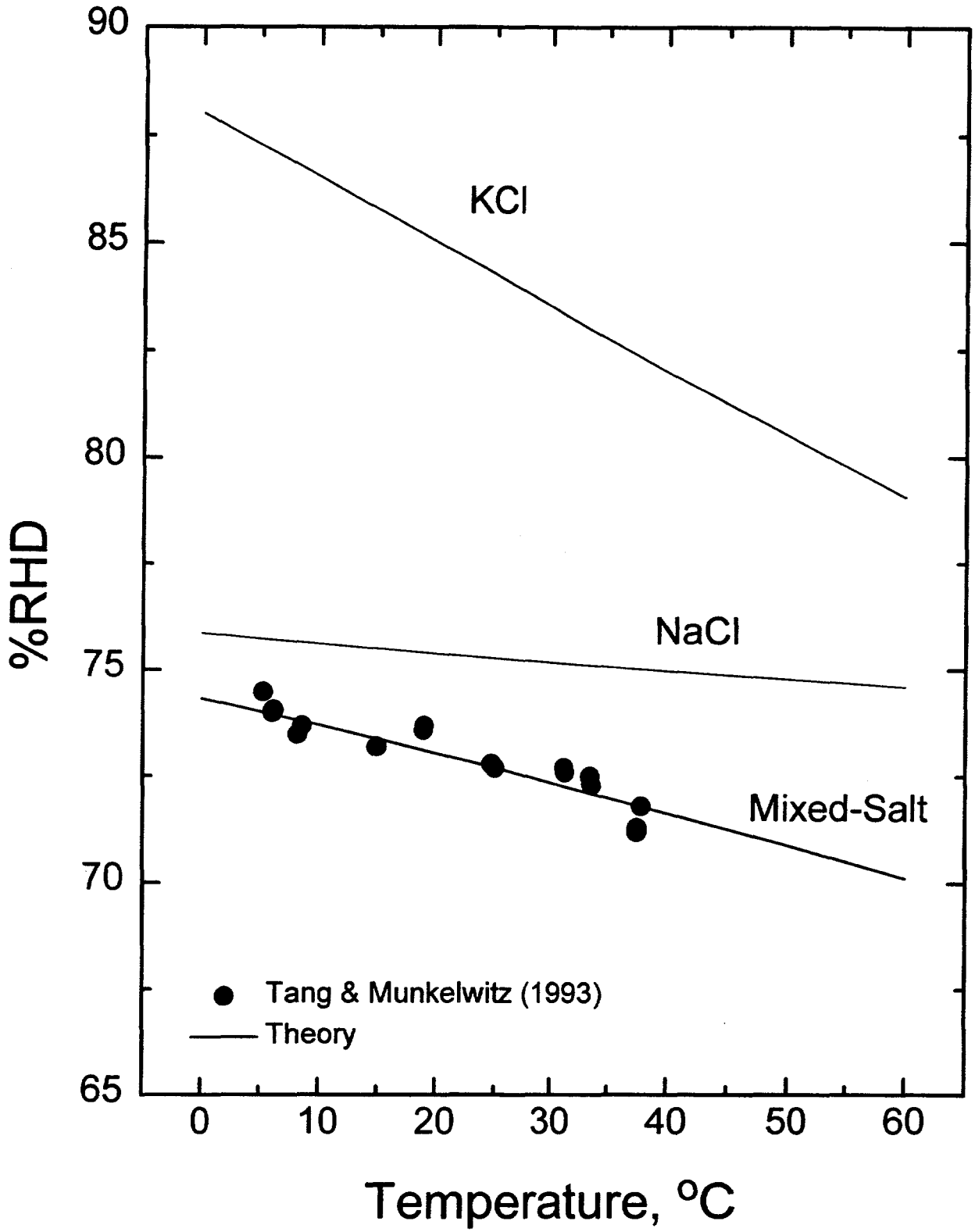
90
85
80
75
70
65
%RHD
KCl
NaCl
Mixed-Salt
Tang & Munkelwitz (1993)
Theory
0
10
20
30
40
50
60
Temperature, °C

Figure 8

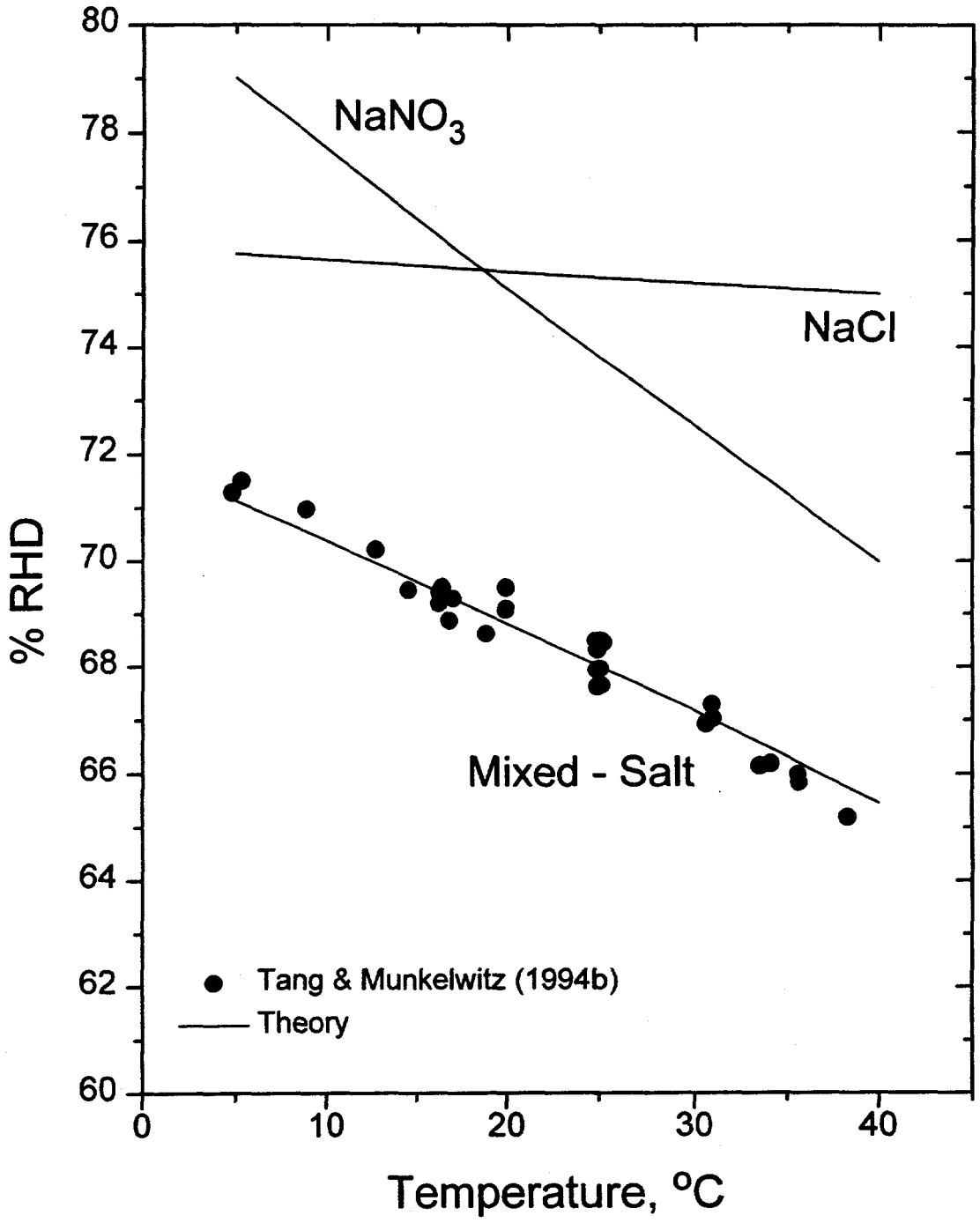
80
78
76
74
72
70
68
66
64
62
60
% RHD
0
10
20
30
40
Temperature, °C
NaNO3
NaCl
Mixed - Salt
Tang & Munkelwitz (1994b)
Theory

Figure 9

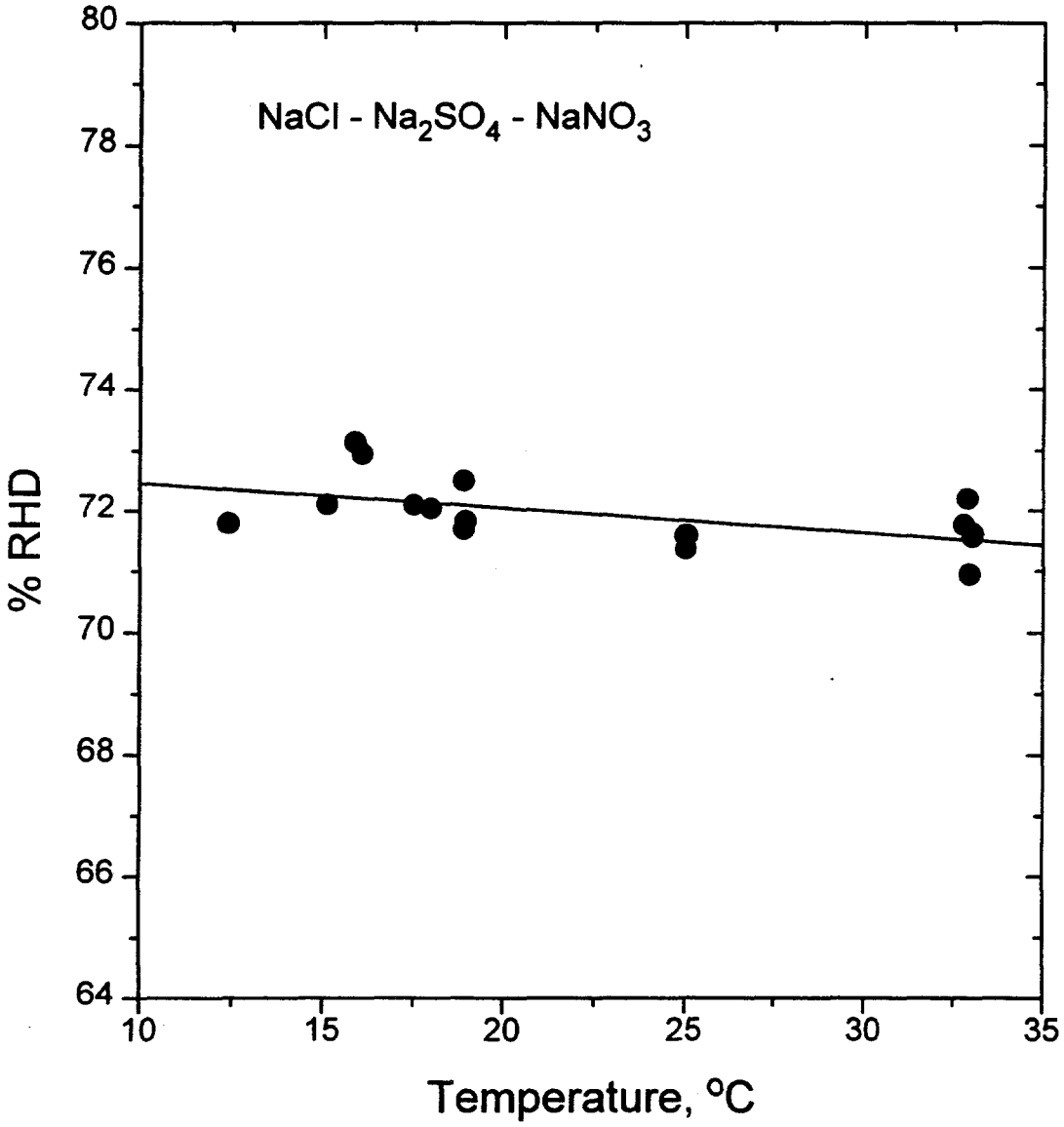
NaCl - Na2SO4 - NaNO3
% RHD
Temperature, °C
80
78
76
74
72
70
68
66
64
10
15
20
25
30
35

Figure 10